Supplementary Information

Design of a Graphene Nitrene Two-Dimensional Catalyst Heterostructure Providing a Well-Defined Site Accommodating One to Three Metals, with Application to CO_2 Reduction Electrocatalysis for the Two-Metal Case

Shiqian Chen[#§], Hao Yuan[#§], Sergey I. Morozov[‡], Lei Ge[§], Li Li[§], Lai Xu*[§], and William A. Goddard III*[†]

§ Institute of Functional Nano & Soft Materials (FUNSOM), Jiangsu Key Laboratory for Carbon-Based Functional Materials & Devices; Soochow University; Suzhou, 215123 (China)

‡ *Department of Physics of Nanoscale systems, South Ural State University, 76 prospect Lenina, Chelyabinsk 454080, Russia*

†*Materials and Process Simulation Center (MSC), California Institute of Technology (Caltech), Pasadena, California, 91125, U.S.A.*

# Contributed equally to this work

Corresponding authors: LX: xulai15@suda.edu.cn; ORCID 0000-0003-2473-3359

WAG: wag@caltech.edu； ORCID 0000-0003-0097-5716

Discussion of Supplementary information

Fig. S2 shows that chemisorbed bent CO_2^- on FeFe-grafiN_6 leads to a bond angle of 126.83° with bond distances of 1.87 Å for Fe-O and 1.94 Å for Fe-C. This leads to charge accumulation near the O atom and electron loss within the C-O bond, indicating that CO_2 is activated. The physical adsorption of CO_2 on CuCu-grafiN_6 remains linear, the distance to the metal is greater than 3Å.

Fig. S3 shows the adsorption at the C_3N part of the framework. The adsorption energy is about -0.21 eV (Table S2). We found that grafiN_6 can promote the initial capture of CO_2, but the main catalytic site remains double metal atom.

Fig. S11a and S11b show chemisorbed bent CO_2^- for both systems, which exhibit a large amount of charge transfer. S11c and S11d show *OCOH after reduction of bent CO_2^-. Additional charge accumulates between the *HCOO intermediate and the metal atoms. This shows the strong interactions of the intermediate with the metal atoms. For *HCOO chemisorption, the charge accumulation between Fe and O atoms is significantly larger than that between Cu and O atoms, demonstrating that the affinity between O and Cu atoms is weaker than that of Fe. Moreover, Fig. S11d shows a larger charge loss between C and O atoms in the Fe-Cu system, indicating better activation of the C-O bond for the Fe-Fe system, resulting in easier reduction of *HCOO compared to *HCOOH. This is also indicated by the LPDOS diagram in Fig.S12. For the Fe-Cu system, the interaction between the orbitals of bimetal-3d and O-2p near the Fermi energy level is stronger than that in the Fe-Fe system. However, Fig. S12c and S12d show that the d orbital and the p orbital are more hybridized in the Fe-Fe system than in the Fe-Cu system, indicating that substituting an Fe atom with Cu atom changes the O adsorption pattern. Therefore, we conclude that the catalytic performance difference between the Fe-Fe system and Fe-Cu system arises mainly from different oxophilic properties of Fe and Cu atoms combined with the difference in ability to provide electrons for the overall catalysis. Of course, substitution of Cu for Fe may adjust the binding state of important intermediates such as *HCOO, making them easier to be further hydrogenated to provide alternate reaction pathways.

Figure S14 considers the structural changes during the transformation, the initial distance of 2.85 Å between the two carbon atoms for Fe-Cu is larger than the 2.44 Å for Fe-Fe. As the transformation proceeds, the distance between the metal atoms and the substrate changes. Therefore, compared with the Fe-Fe system coupling requires 0.64 eV, the Fe-Cu system requires an energy barrier of 0.80 eV to react. And for FeCu, it is also very difficult to generate C-C coupled pre-product *COH, which requires an external potential of -0.92 V. Therefore, the Fe-Cu system is less likely to yield C2 products from this pathway.

Figure captions

Table Captions

Videos

Video S1. Fe-Fe heating from 20 K to 1000 K over 10 ps

https://yadi.sk/i/7MFAyaaFhAWZkg

https://yadi.sk/i/offymT2fdDbrFw

https://yadi.sk/i/U9_mJQANjnKnIw

Video S2. Fe-Cu heating from 20 K to 1000 K over 10 ps

https://yadi.sk/i/LR0F6WCr9jlB3A

https://yadi.sk/i/qxNPRnQECn3pKw

https://yadi.sk/i/M_N1ZsaLaQptvg

Video S3. Fe-Fe cooling from 1000 K to 300 K over 7 ps

https://yadi.sk/i/kLTf2SWaWK4t0A

https://yadi.sk/i/zYCa626Wevtw9Q

https://yadi.sk/i/ar2FpNMxNzAIRw

Video S4. Fe-Cu cooling from 1000 K to 300 K over 7 ps

https://yadi.sk/i/11xu181Enkuw0Q

https://yadi.sk/i/_C7NArxa8QL5Dw

https://yadi.sk/i/VbZZgSnaNZB_JA

Video S5. Fe-Fe holding 300 K over 3 ps

https://yadi.sk/i/4LgpLvL6xCgkxQ

https://yadi.sk/i/aLhmPnItfEwHQ

https://yadi.sk/i/sTS1Me2o4O1JLA

Video S6. Fe-Cu holding 300 K over 3 ps

https://yadi.sk/i/kugirL2qeVns2w

https://yadi.sk/i/XrVNRRcQsHHG_A

https://yadi.sk/i/PlrUJdwYHPQifA

Table S1. The thermodynamic data for the molecules considered in this paper. (Pressure = 1 bar)

	E (eV)	ZPE (eV)	TS (eV)	G (eV)
H_2 (g)	-6.76	0.28	0.40	-6.88
H_2O (l)	-14.23	0.57	0.67(g)	-14.33
CO (g)	-14.80	0.13	0.61	-15.27
CO_2 (g)	-22.99	0.30	0.66	-23.35
CH_3OH (l)	-30.22	1.39	0.74(g)	-29.61
CH_4 (g)	-24.03	1.22	0.58	-23.39
C_2H_4 (g)	-31.98	1.37	0.56	-31.17
CH_3CH_2OH(g)	-46.92	2.11	0.87	-45.68

Table S2. Adsorption energy of CO_2 on Fe-Fe and Fe-Cu systems. (corresponding sites are shown in Fig. S3)

Adsorption site	ΔE_{ads} (eV)
1	-0.21
2	-0.22
3	-0.21
4	-0.21

Table S3. The H_2 evolution reaction (HER) and Gibbs free energy change of the first protonation step in the CO_2 reduction reaction (CRR) in eV.

	ΔG_{H^*}	ΔG_{COOH^*}	ΔG_{HCOO^*}
Fe-Fe	-0.44	-0.39	-0.85
Fe-Cu	0.28	-0.01	-0.31
Fe-Pd	-0.24	0.59	-0.32
Fe-Co	-1.41	0.23	0.23
Co-Co	-0.47	0.21	-0.22
Ni-Ni	-0.49	0.16	-0.04
Co-Cu	-0.73	0.03	-0.40
Pd-Co	-0.07	0.41	0.16
Pd-Cu	-0.45	0.40	0.01
Fe-Ni	-0.49	0.06	-0.03
Co-Ni	-0.47	0.49	-0.06
Ni-Cu	-0.63	0.57	0.06
Pd-Ni	-0.08	0.49	0.21
Cu-Cu	-0.74	-0.37	-0.88
Pd-Pd	0.18	0.49	0.01

Table S4. Specific values of the free energy change at each step involved in the Fe-Fe and Fe-Cu systems in Figure 2.

Reaction process	Fe-Fe (eV)	Fe-Cu (eV)
$*CO_2 + H^+ \rightarrow *COOH$	-0.39	-0.01
$*CO_2 + H^+ \rightarrow *HCOO$	-0.85	-0.31
$*COOH + H^+ \rightarrow *CO + H_2O$	-0.38	-0.66
$*HCOO + H^+ \rightarrow *HCOOH$	0.88	0.68
$*CO + H^+ \rightarrow *CHO$	0.55	0.90
$*CO + H^+ \rightarrow *COH$	0.43	0.92
$*COH + H^+ \rightarrow *C + H_2O$	1.09	0.84
$*COH + H^+ \rightarrow *CHOH$	0.52	-0.12
$*CHO + H^+ \rightarrow *CHOH$	0.40	-0.10
$*CHO + H^+ \rightarrow *CH_2O$	-0.35	-0.30
$*CHOH + H^+ \rightarrow *CH + H_2O$	-0.16	0.25
$*CHOH + H^+ \rightarrow *CH_2OH$	-0.59	-0.21
$*CH_2O + H^+ \rightarrow *CH_3O$	-0.21	-0.39
$*CH + H^+ \rightarrow *CH_2$	-0.61	-0.71
$*CH_2OH + H^+ \rightarrow *CH_3OH$	-0.10	0.08
$*CH_3O + H^+ \rightarrow *O + CH_4$	-1.42	-0.79
$*CH_2 + H^+ \rightarrow *CH_3$	-0.79	-0.61
$*O + H^+ \rightarrow *OH$	-0.21	-0.53
$*CH_3 + H^+ \rightarrow *CH_4$	0.93	0.40
$*OH + H^+ \rightarrow *H_2O$	0.61	0.48

Table S5. Adsorption energy of various products on Fe-Fe and Fe-Cu systems.

System	$*CH_3OH$	$*CH_4$
Fe-Fe	-1.16	0.35
Fe-Cu	-1.12	-0.20

Table S6. Specific values of the free energy change at each step involved in the Fe-Fe systems in Figure 4.

Reaction process	Fe-Fe （eV）
*COH + CO(g) → *COH + *CO	-0.52
*COH + *CO → *COHCO	0.68
*COHCO + H^+ → *COHCOH	0.34
*COHCOH + H^+ → *CCOH+H_2O	-0.32
*CCHO + H^+ → *CHCOH	-0.42
*CHCOH + H^+ → *CCH+H_2O	0.28
*CHCOH + H^+ → *CHCHOH	-0.83
*CCH + H^+ → *CCH_2	0.03
*CHCHOH + H^+ → *CH_2CHOH	-0.33
*CCH_2 + H^+ → *$CHCH_2$	-0.89
*CH_2CHOH + H^+ → *CH_3CHOH	0.56
*$CHCH_2$ + H^+ → *CH_2CH_2	-1.21
*CH_3CHOH + H^+ → *CH_3CH_2OH	0.13

Table S7. Specific values of the free energy change at each step involved in the Fe-Cu systems in Figure 6.

Reaction process	Fe-Cu （eV）
CH_2+CO(g) →CH_2 + *CO	0.05
*CH_2 + *CO → *CH_2CO	-0.12
*CH_2CO + H^+ → *CH_2COH	-0.81
*CH_2COH + H^+ → *CCH_2	0.19
*CH_2COH + H^+ → *CH_2CHOH	0.04
*CCH_2 + H^+ → *CH_2CH	-0.85
*CH_2CHOH + H^+ → *CH_3CHOH	0.08
*CH_2CH + H^+ → *CH_2CH_2	-0.25
*CH_3CHOH + H^+ → *CH_3CH_2OH	0.17

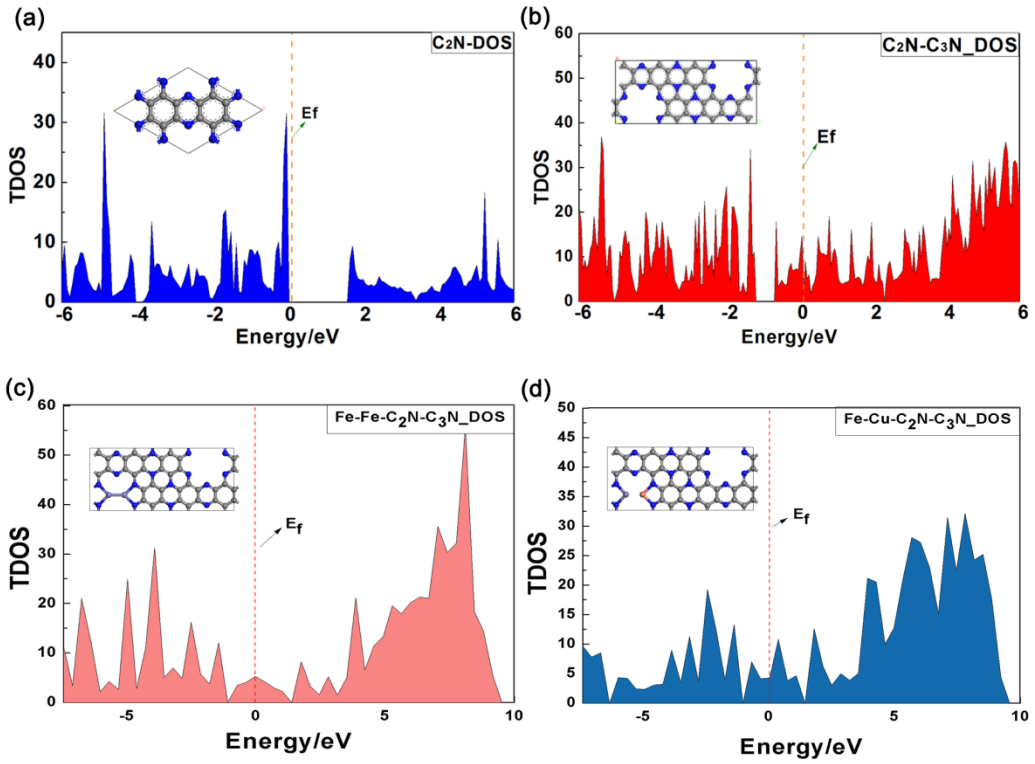

Figure S1. (a)The density of states on pure C_2N (Reproduced with permission from Reference[1]) (b) The density of states on coplanar C_2N-C_3N. (Reproduced with permission from Reference[1]) (c) The density of states on FeFe-GrafiN_6 (d) The density of states on FeCu-GrafiN_6

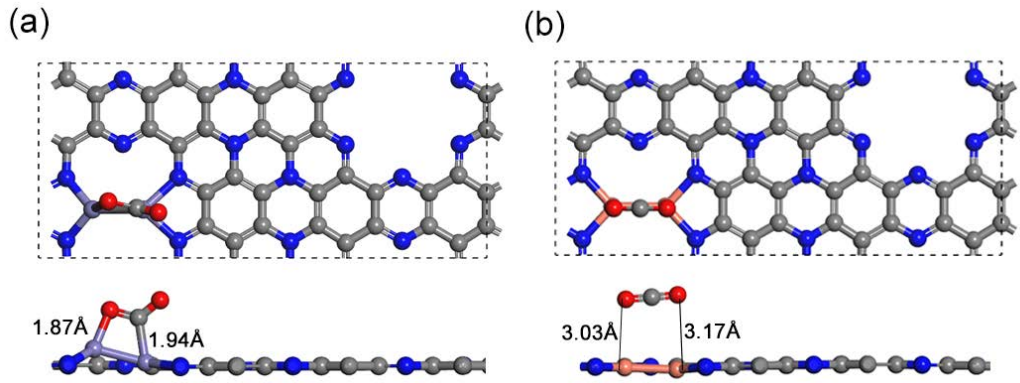

Figure S2. Binding site for CO_2 on FeFe-grafiN_6, (a) chemisorbed CO_2^- on the FeFe-grafiN_6, and (b) physisorbed linear CO_2 on CuCu-grafiN_6

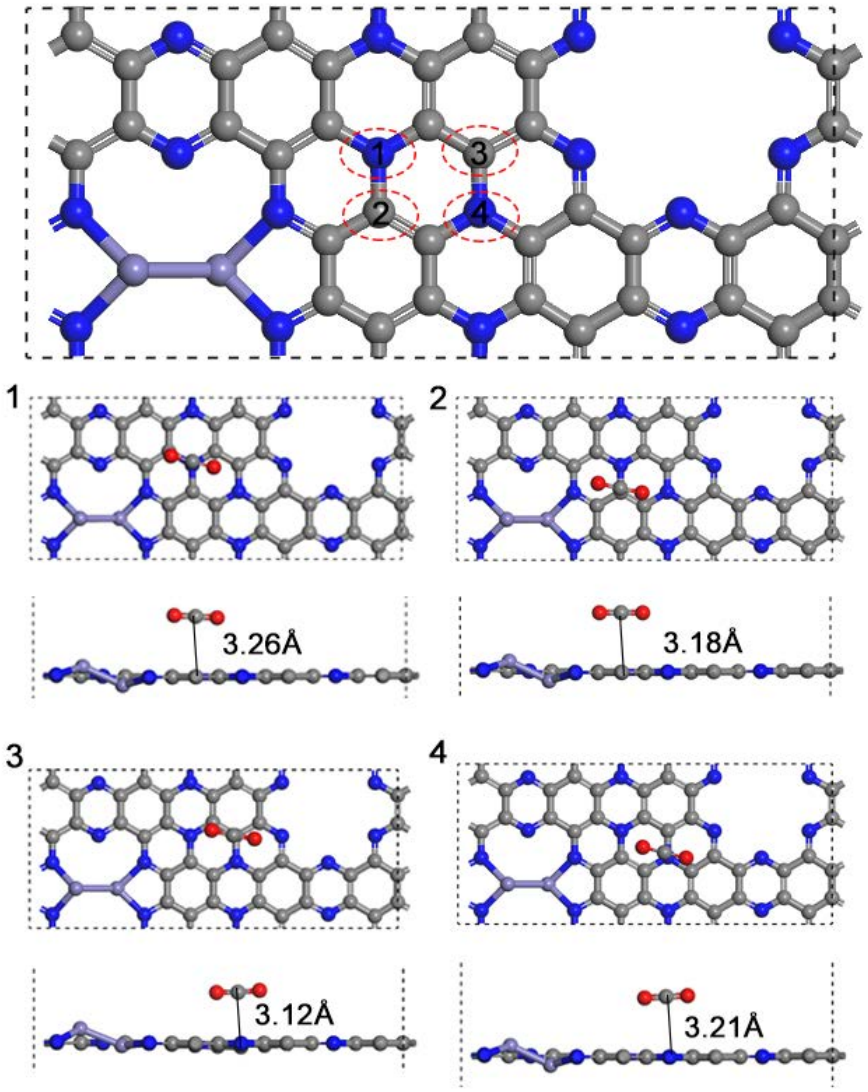

Figure S3. Top view and side view of the CO_2 physisorption on the FeFe-grafiN_6 framework

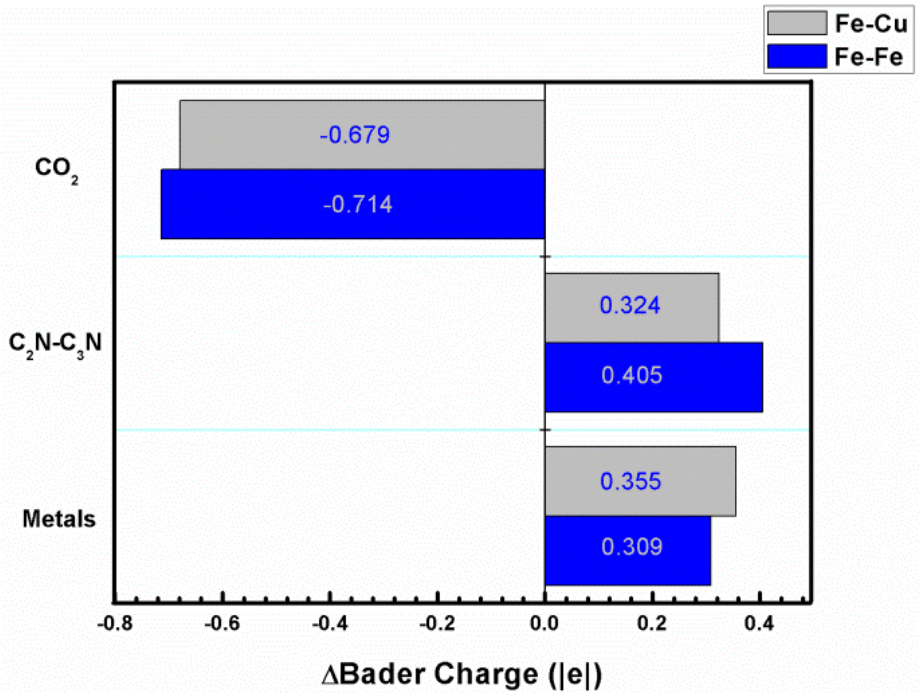

Figure S4. The Bader charge changes of the metal atoms, grafiN_6 substrate, and CO_2 intermediates. The Bader charge of CO_2 is 0.

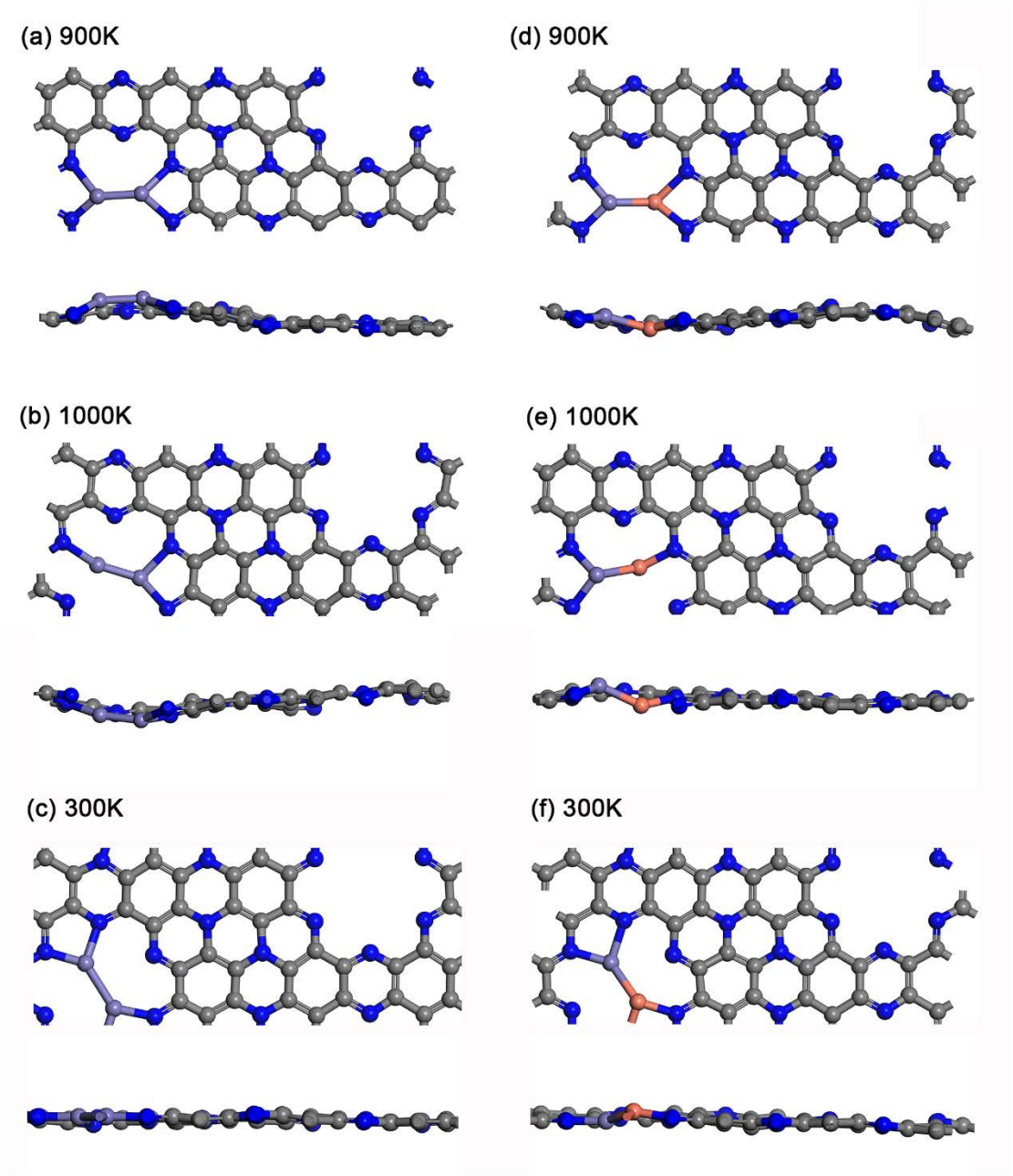

Figure S5. Snapshots during 10 ps heating of FeFe-GrafiN$_6$ and FeCu-GrafiN$_6$ from 20 to 1000 K.

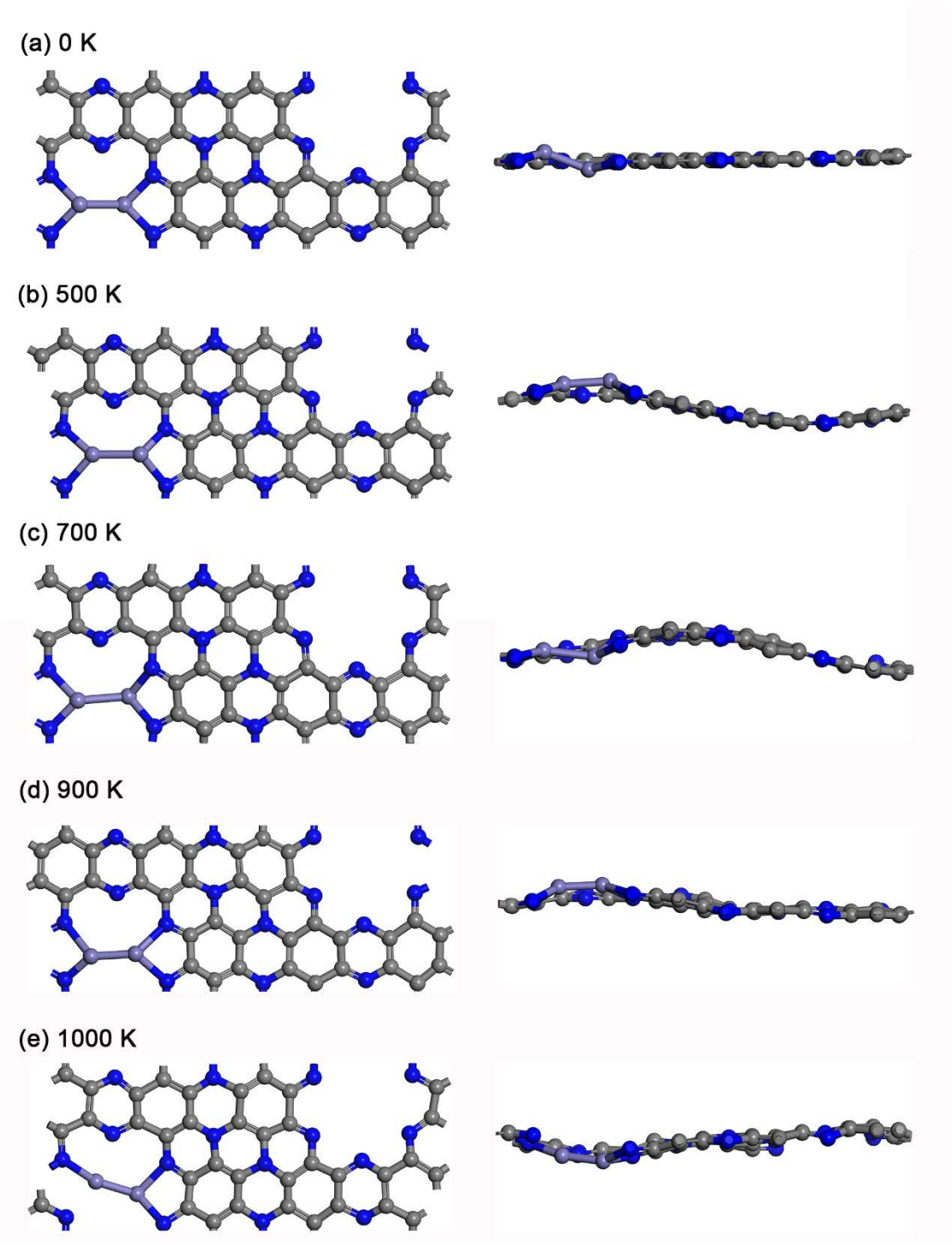

Figure S6. Snapshots during 10 ps heating of FeFe-GrafiN_6 from 20 to 1000 K.

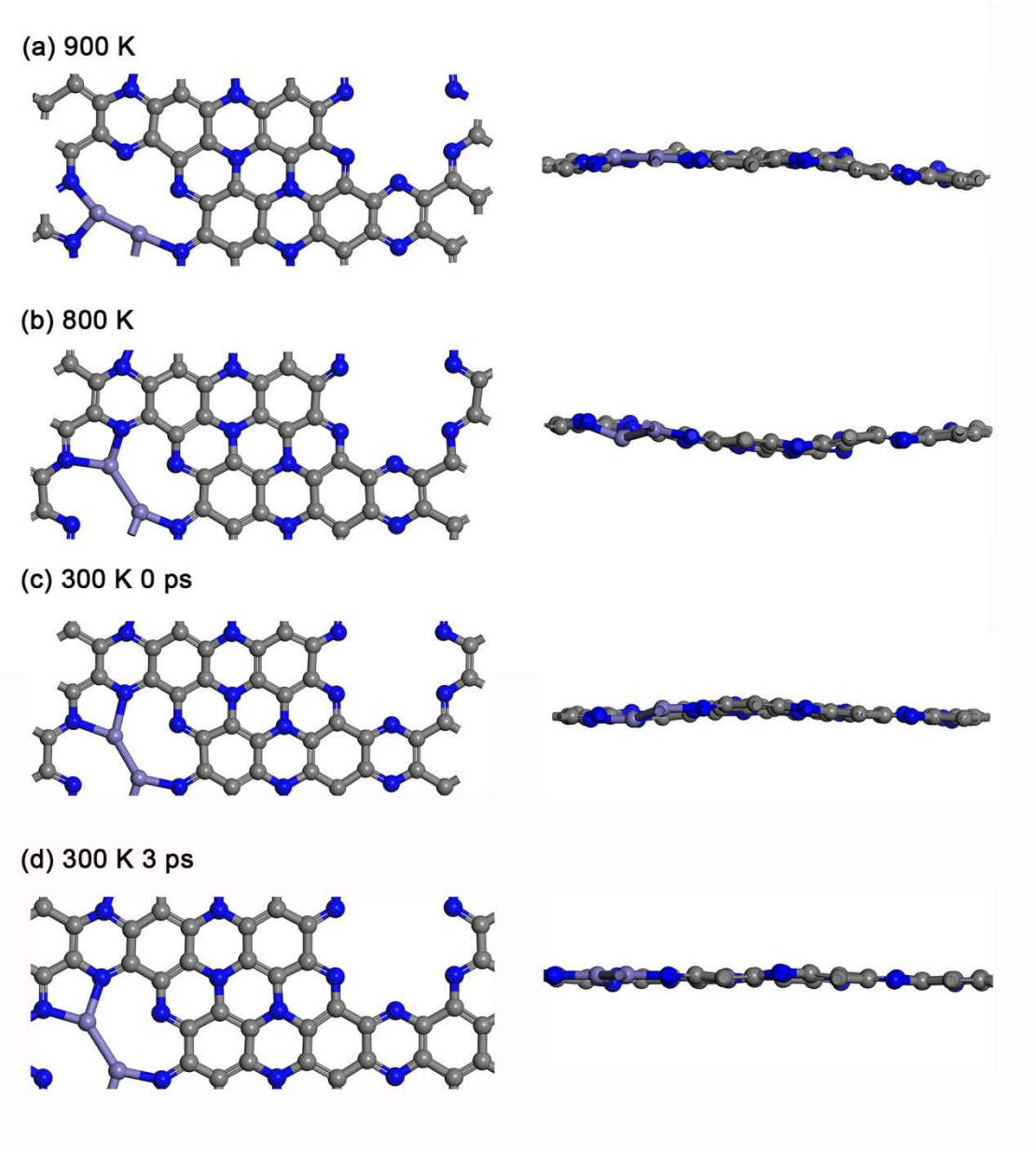

Figure S7. Snapshots during 7 ps cooling of FeFe-GrafiN_6 from 1000 K to 300 K and holding at 300K for 3ps.

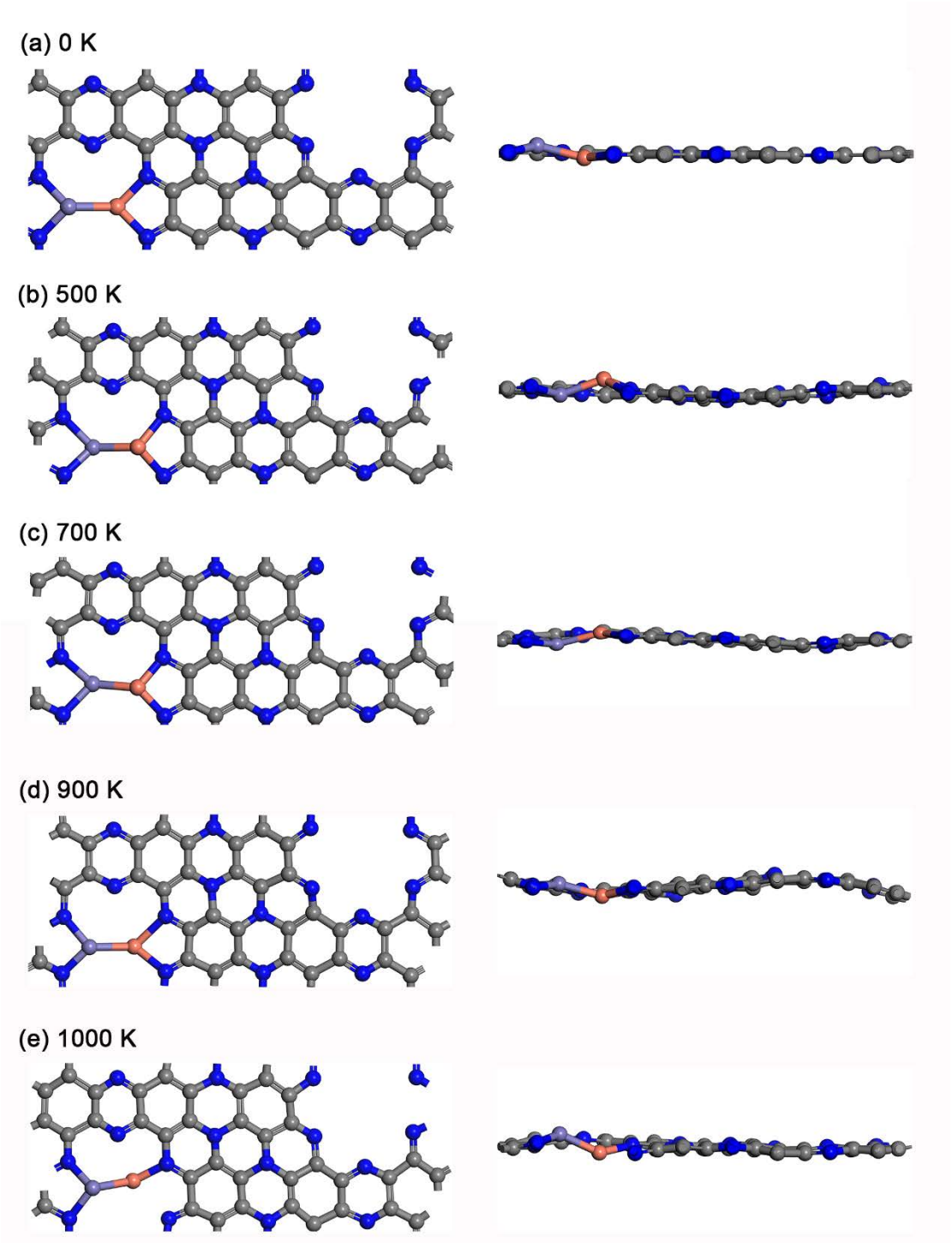

Figure S8. Snapshots during 10 ps heating of FeCu-GrafiN$_6$ from 20 to 1000 K.

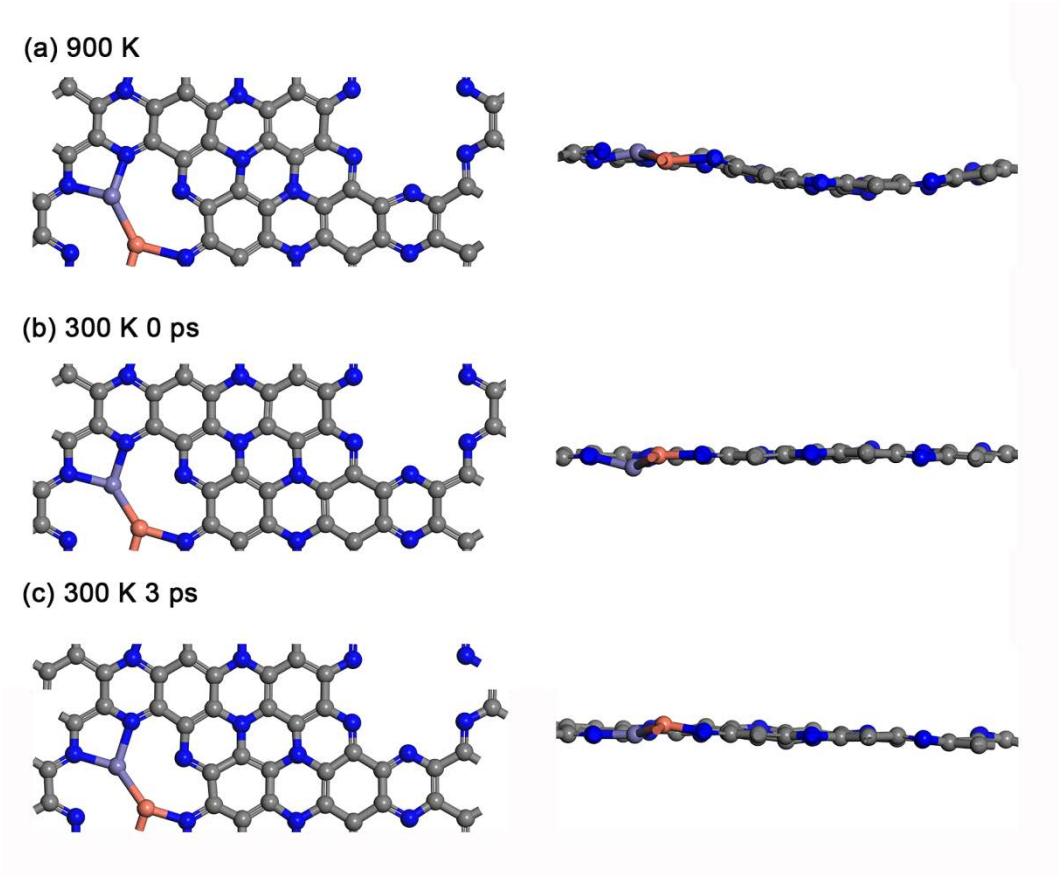

Figure S9. Snapshots during 7 ps cooling of FeCu-GrafiN$_6$ from 1000 K to 300 K and holding at 300K for 3ps.

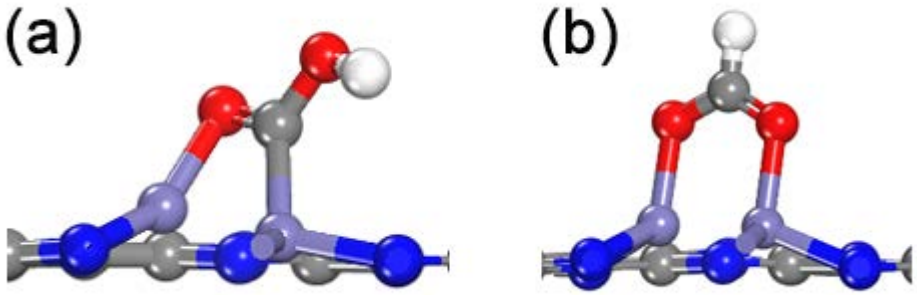

Figure S10. (a) chemisorbed *OCOH on FeFe-grafiN$_6$ (b) chemisorbed *HCOO on FeFe-grafiN$_6$.

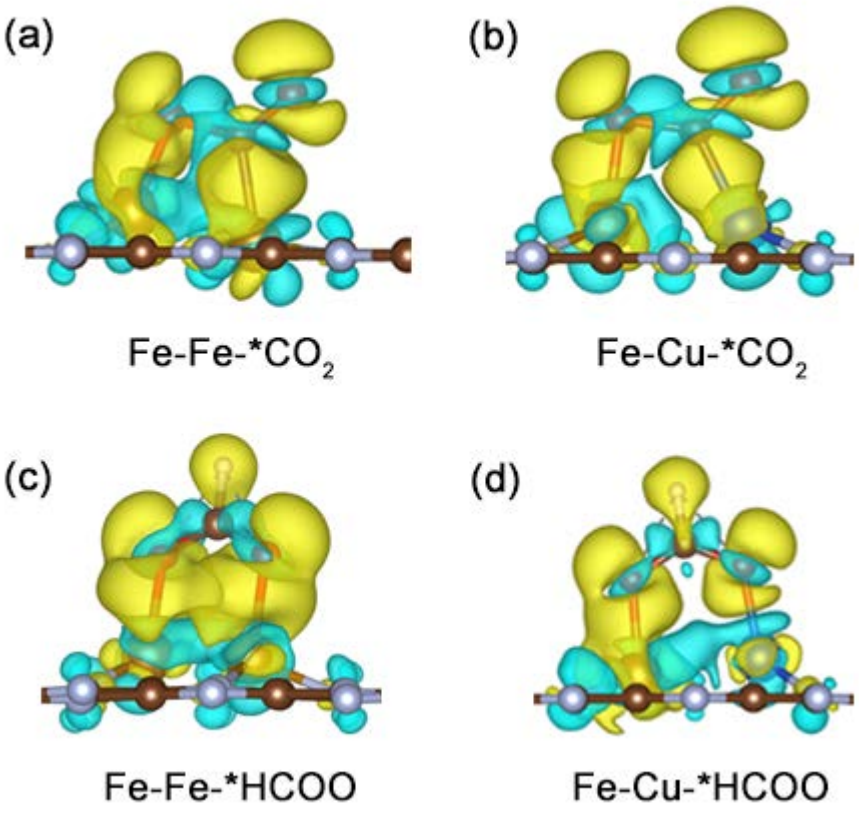

Figure S11. The charge density difference of (a) bent $*CO_2^-$ on FeFe-grafiN_6 (b) bent $*CO_2^-$ on FeCu-grafiN_6 (c) *HCOO on FeFe-grafiN_6 (d) *HCOO on FeFe-grafiN_6. Yellow zones represent charge accumulation and blue zones represent charge depletion.

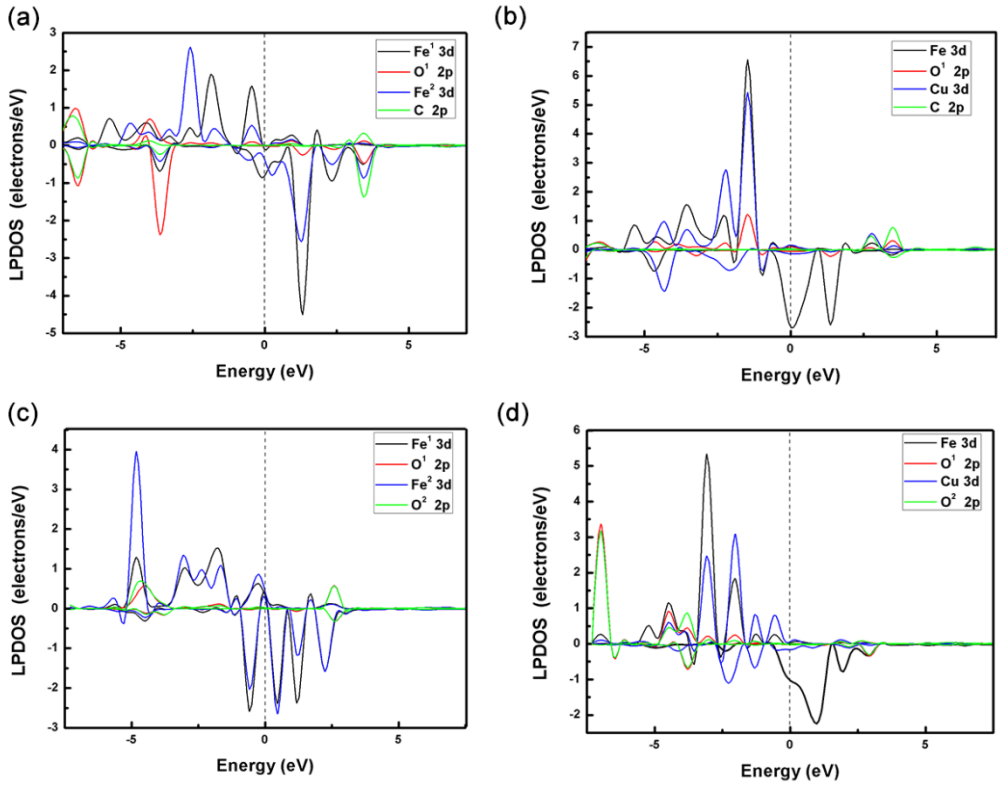

Figure S12. The local partial density of states (LPDOS) of bent $*CO_2^-$ chemisorbed on (a) FeFe-grafN$_6$ and (b) FeCu-grafN$_6$. The LPDOS of *HCOO chemisorbed on (c) FeFe-grafN$_6$ and (d) FeCu-grafN$_6$. The location of the atom represented in the figure is shown in Figure S20.

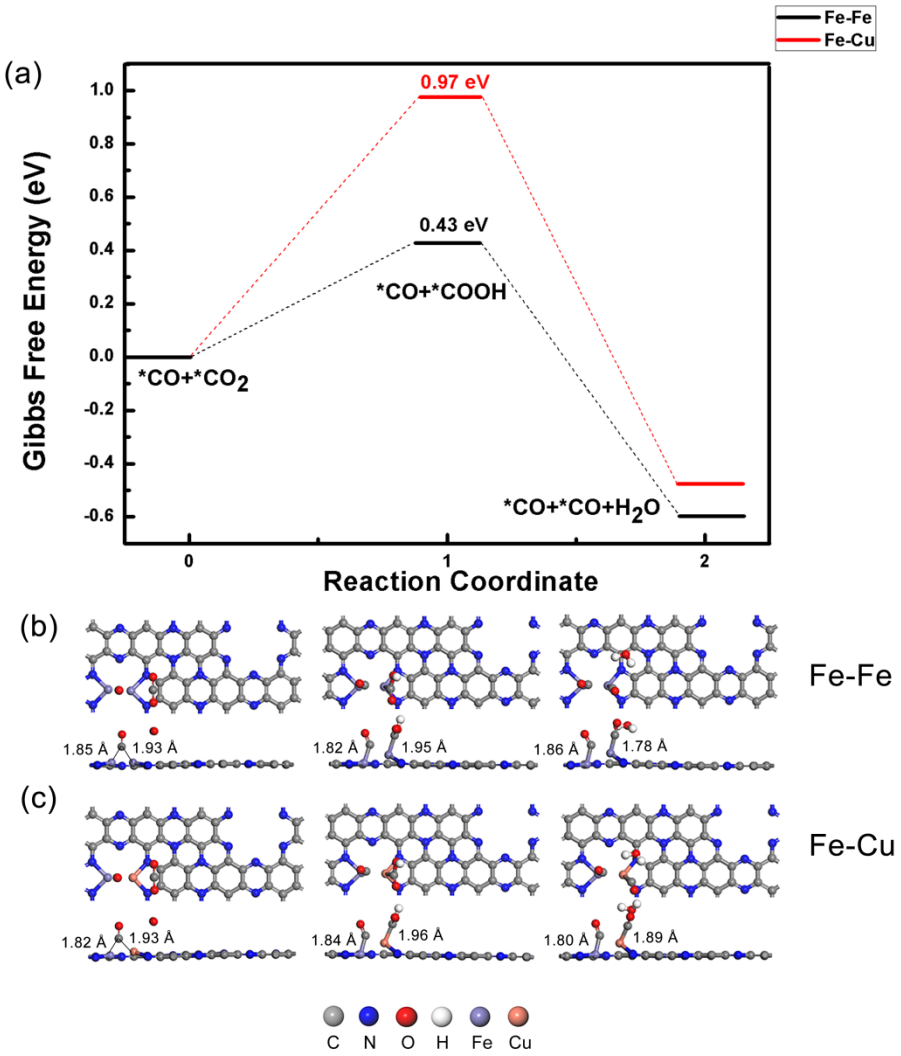

Figure S13. (a) The *CO+*CO_2→*CO+*COOH→*CO+*CO+H_2O reaction free energy change in two systems. （b-c）The conversion of another molecule of CO_2 to CO in (b)Fe-Fe, (c)Fe-Cu, from left to right, *CO+*CO_2, *CO+*COOH, *CO+*CO+H_2O.

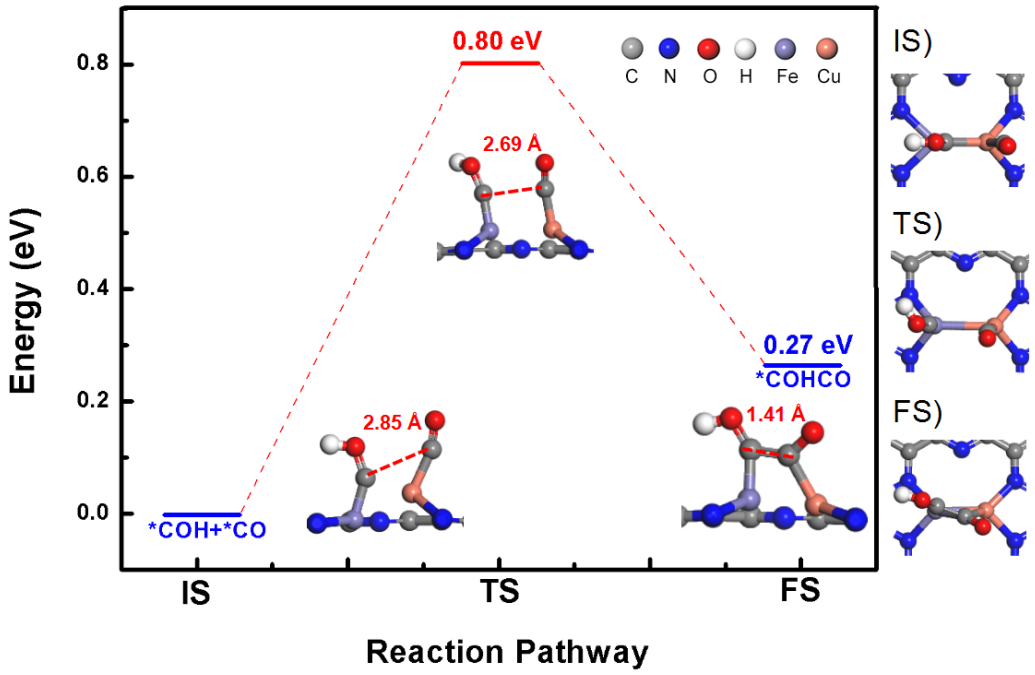

Figure S14. The structure diagrams and energy changes involved in the reaction*CO+*COH→*COCOH for FeCu-grafiN$_6$ system.

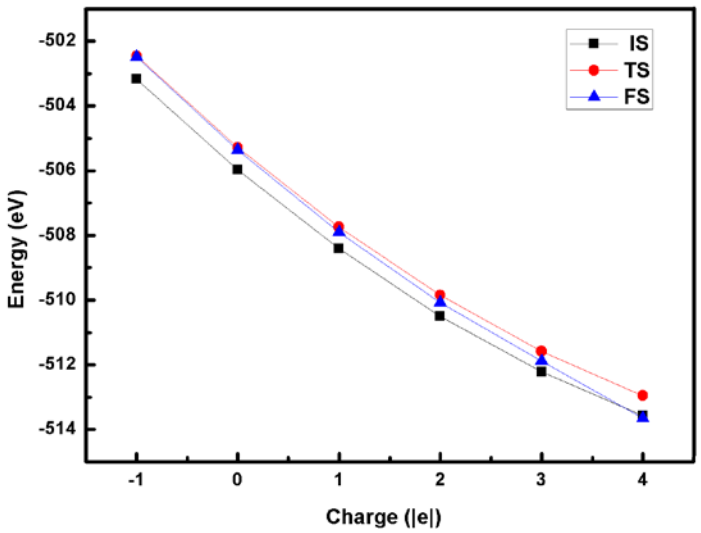

Figure S15. Energy change trend of C-C coupling IS, TS and FS with different charges in Fe-Fe System. (IS:*COH+*CO, FS:*COHCO).

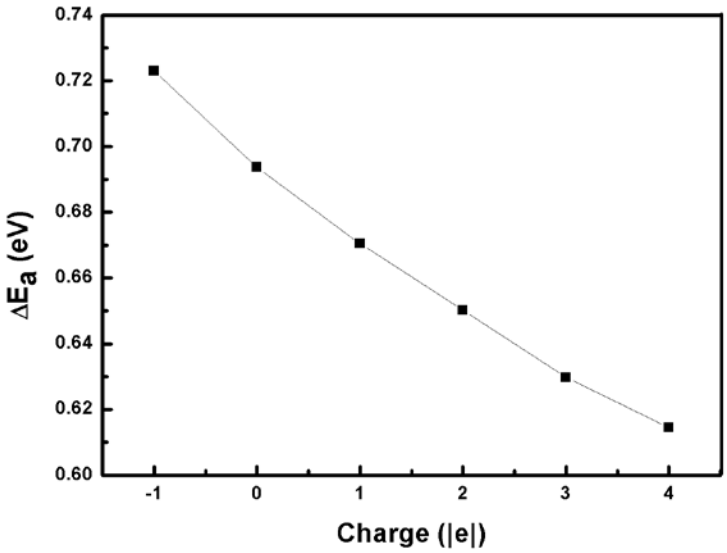

Figure S16. Change trend of C-C coupling reaction energy barrier in Fe-Fe system with different charges in the system.

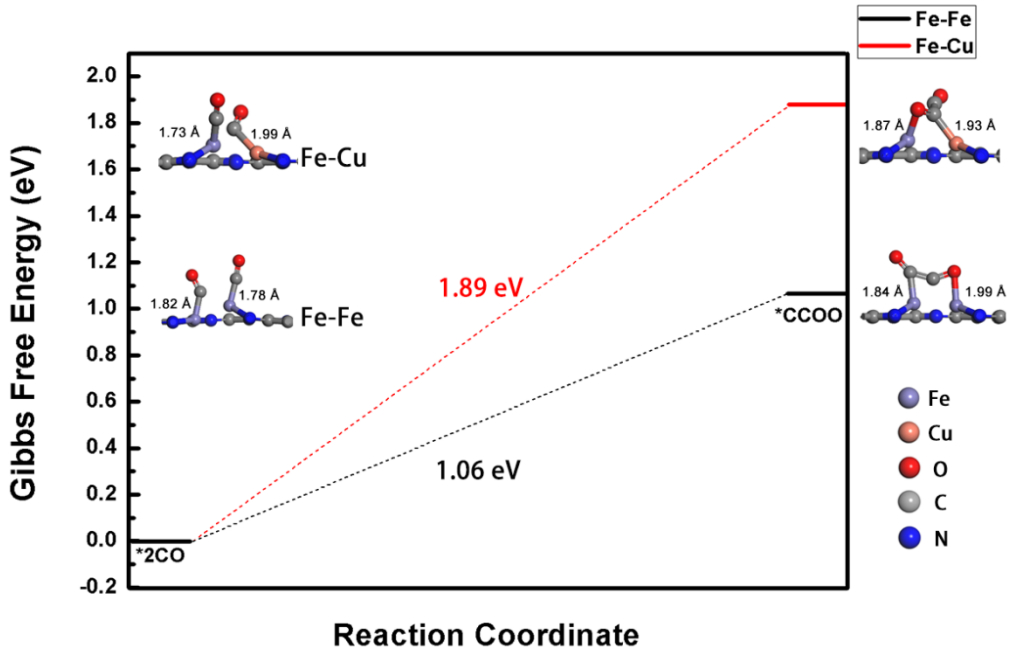

Figure S17. The free energy changes for the process of transforming two chemisorbed CO* to OCCO* in FeFe-grafiN_6 and FeCu grafiN_6 systems. The structural parameters are shown for *OCCO on both catalysts.

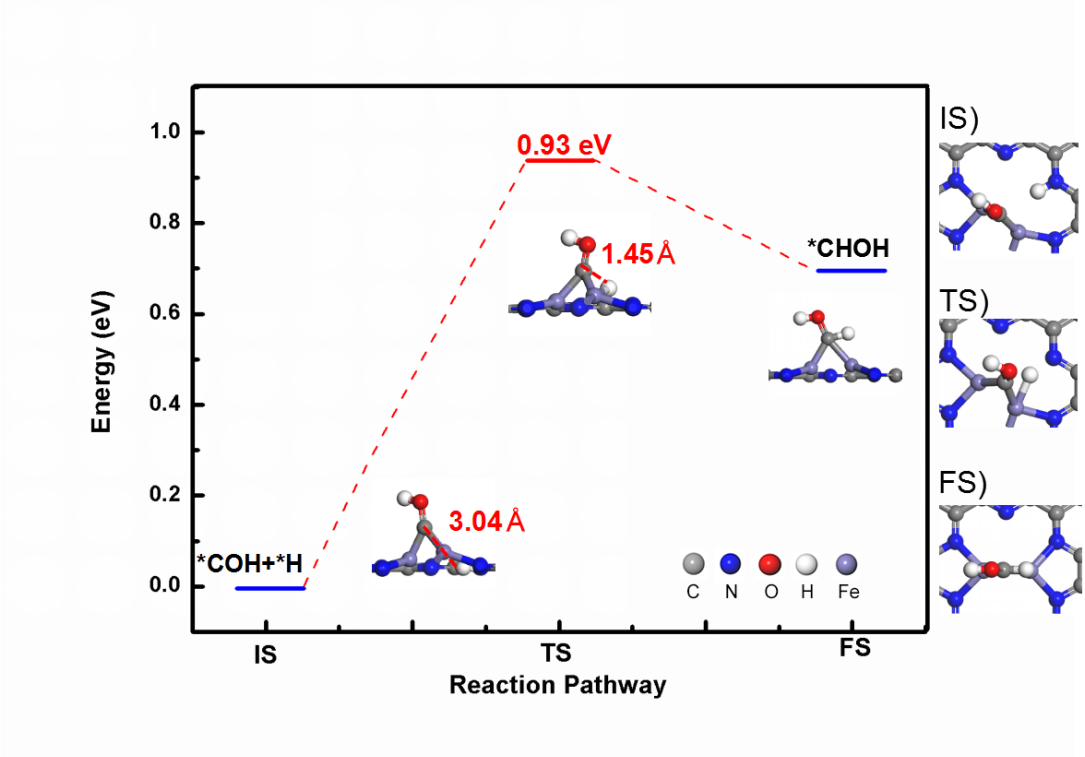

Figure S18. The structure diagrams and energy changes involved in the reaction*COH+*H→*CHOH for FeFe-grafiN$_6$ system.

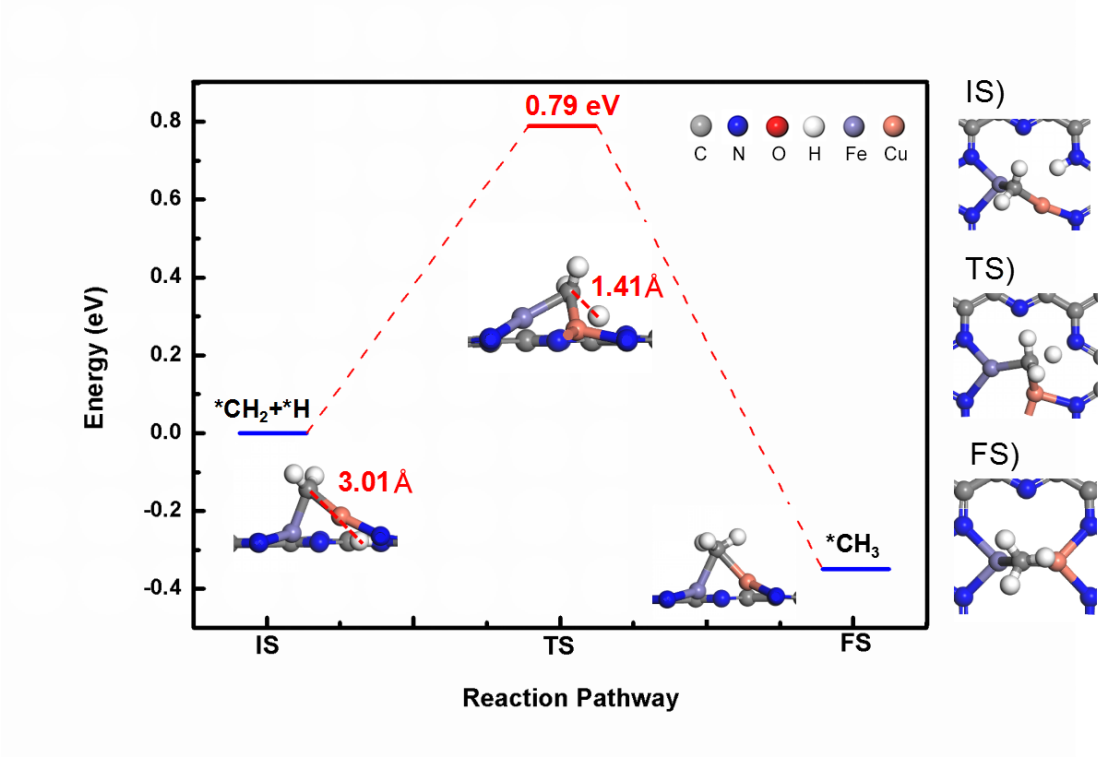

Figure S19. The structure diagrams and energy changes involved in the reaction*CH_2+*H→*CH_3 for FeCu-grafiN_6 system.

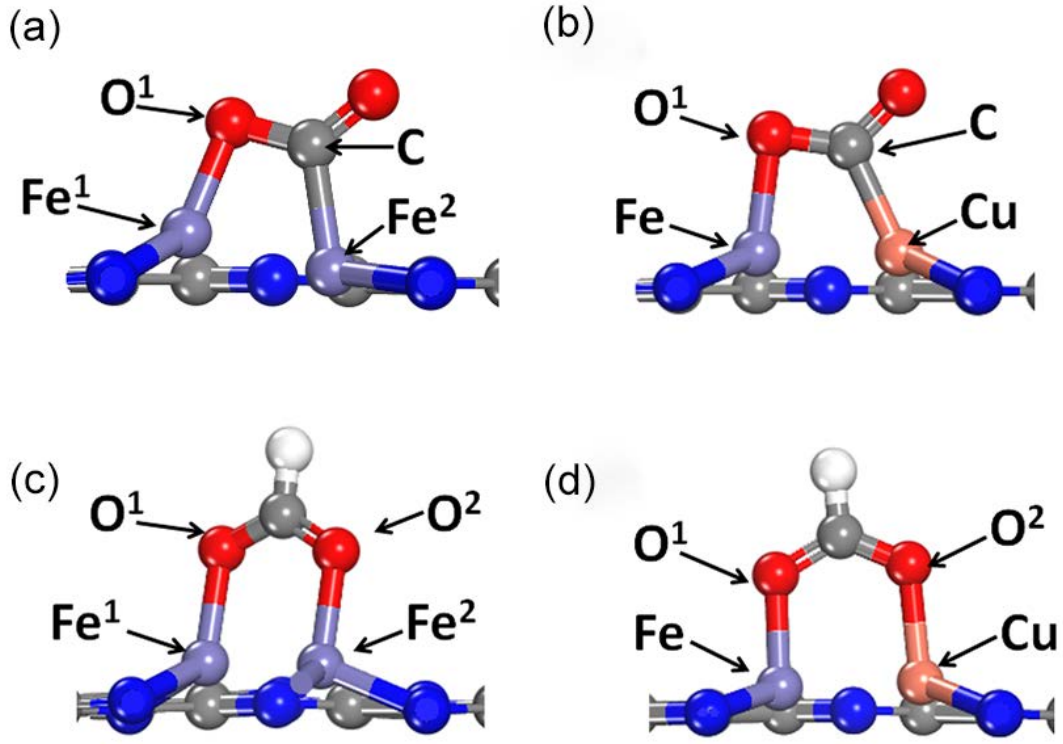

Figure S20. The position of the specific atoms represented in the LPDOS of Figure S10. Bent *CO_2^- chemisorbed on (a) FeFe-grafN$_6$ and (b) FeCu-grafN$_6$. *HCOO chemisorbed on (c) FeFe-grafN$_6$ and (d) FeCu-grafN$_6$.

References

(1) Xu, W.; Chen, C.; Tang, C.; Li, Y.; Xu, L. Design of Boron Doped C2N-C3N Coplanar Conjugated Heterostructure for Efficient HER Electrocatalysis. *Sci. Rep.-UK* **2018**, *8* (1), 5661.